ADVANCED ENERGY MATERIALS

Supporting Information

for *Adv. Energy Mater.,* DOI: 10.1002/aenm.201803440

Dopant-Dependent Stability of Garnet Solid Electrolyte Interfaces with Lithium Metal

*Yisi Zhu, Justin G. Connell, Sanja Tepavcevic, Peter Zapol, Regina Garcia-Mendez, Nathan J. Taylor, Jeff Sakamoto, Brian J. Ingram, Larry A. Curtiss, John W. Freeland, Dillon D. Fong, and Nenad M. Markovic**

Supporting Information

Dopant-Dependent Stability of Garnet Solid Electrolyte Interfaces with Lithium Metal

Yisi Zhu[1], Justin G. Connell[1,2], Sanja Tepavcevic[1], Peter Zapol[1], Regina Garcia-Mendez[3], Nathan J. Taylor[4], Jeff Sakamoto[3,4], Brian J. Ingram[4], Larry A. Curtiss[1], John W. Freeland[5], Dillon D. Fong[1], Nenad M. Markovic[1,*]

[1] Materials Science Division, Argonne National Laboratory, Argonne, IL 60439, USA

[2] Joint Center for Energy Storage Research, Argonne National Laboratory, Argonne, IL 60439, USA

[3] Department of Materials Science and Engineering, University of Michigan, Ann Arbor, MI 48109, USA

[4] Department of Mechanical Engineering, University of Michigan, Ann Arbor, MI 48109, USA

[5] Chemical Sciences and Engineering Division, Argonne National Laboratory, Lemont, Illinois 60439, United States

[6] X-ray Sciences Division, Argonne National Laboratory, Argonne, IL 60439, USA

* Email: nmmarkovic@anl.gov

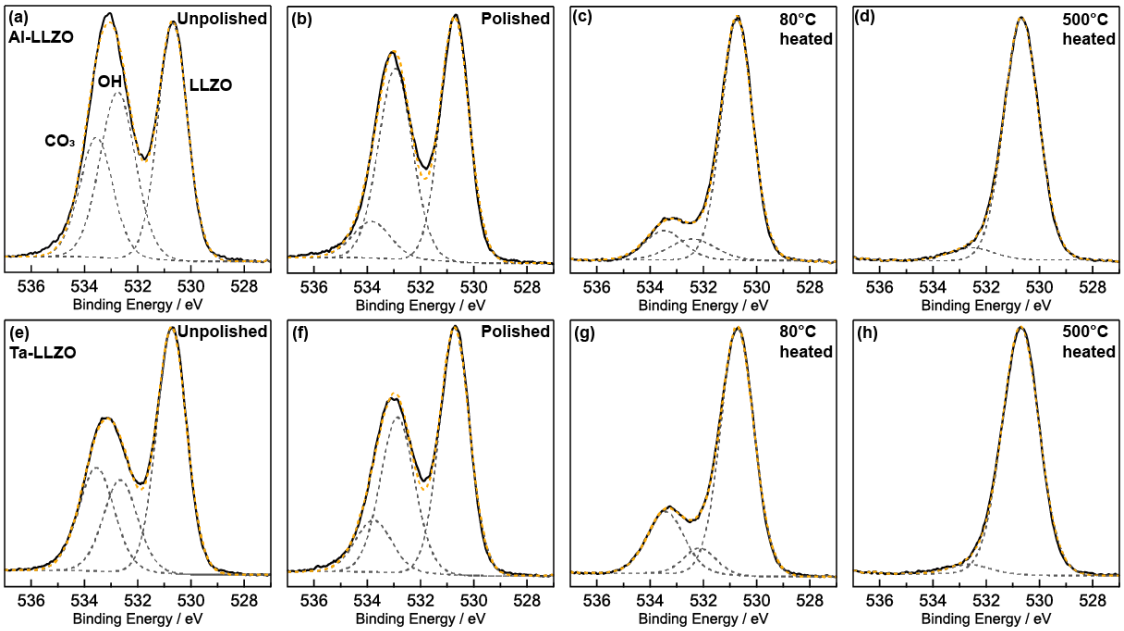

Figure S1. Representative O 1s core level XPS spectra from (a) unpolished (b) polished (c) 80°C UHV heated and (d) 500°C UHV heated, Al-doped LLZO surfaces; and (e) unpolished (f) polished (g) 80°C UHV heated and (h) 500°C UHV heated, Ta-doped LLZO surfaces.

Figure S1 shows XPS O 1s core levels of four distinct surfaces (unpolished, polished, heated to 80°C and heated to 500°C in UHV) for both Al doped and Ta doped LLZO. Each spectrum is deconvoluted into main LLZO peak at 530.7 eV, carbonate peak at 533.7 eV and hydroxyl peak at 532.8 eV. As for Nb-doped material, note that the binding energies for both carbonate and hydroxyl species are ~2 eV higher than their literature values due to differential charging (see Experimental Methods and Figure S3 for more details). Similar to results for Nb doped LLZO (Figure 1), unpolished surfaces (Figure S1a,e) have significant Li_2CO_3 and LiOH content. Polished samples (Figure S1b,f) reveal that much of the carbonate content is removed upon

polishing, but significant LiOH content remains from either the glove box environment or the polishing paper. Heating at low temperature (~80°C) removes most of the hydroxyl species, and UHV heating at 500°C completely removes all Li_2CO_3 and LiOH species, yielding a pristine LLZO surface. The relative LiOH, Li_2CO_3 and LLZO contributions to the O 1s spectra for various surface treatments from Nb doped LLZO (shown in Fig. 1), Al doped LLZO (Fig. S1a-d) and Ta doped LLZO (Fig. S1e-h) are summarized in Table S1.

Table S1. Percentage of various oxygen species on the LLZO for Nb-, Al- and Ta-doped LLZO after different surface treatments. Relative concentrations are calculated from deconvoluted XPS O 1s core level peak intensities in Figures 1 and S1.

Samples				Concentration [at%]		
Unpolished	Polished	80°C	500°C	Li_2CO_3	LiOH	LLZO
$Li_{6.25}Al_{0.25}La_3Zr_2O_{12}$				25.3	34.7	40.0
				10.1	43.3	46.6
				18.2	4.2	77.6
				0.0	4.5	95.5
$Li_{6.5}La_3Zr_{1.5}Nb_{0.5}O_{12}$				23.7	35.0	41.3
				9.3	43.0	47.7
				11.8	9.9	78.3
				0.0	6.6	93.4
$Li_{6.5}La_3Zr_{1.5}Ta_{0.5}O_{12}$				26.7	22.2	51.1
				12.1	37.0	50.9
				20.3	7.2	72.5
				0.0	3.7	96.3

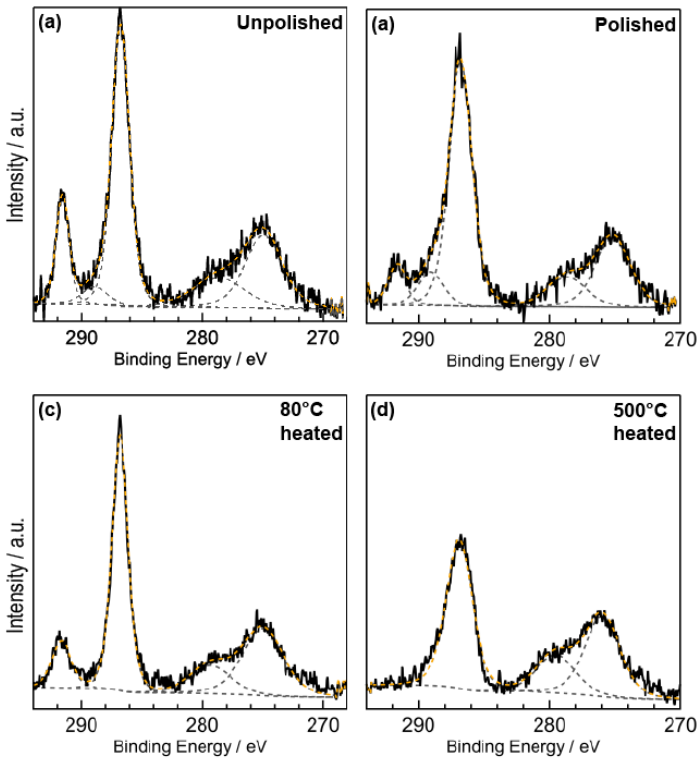

Figure S2. Representative XPS C 1s core level spectra from Nb-doped LLZO with different surface treatments shows relative concentration of carbonate and carbon sp^3 species for (a) unpolished (b) polished (c) 80°C UHV heated and (d) 500°C UHV heated.

The C 1s spectra are deconvoluted and assigned as follows: sp^3 (286.8 eV), C-O-C (289 eV) and Li_2CO_3 (291.6 eV). Binding energy numbers are ~ 2 eV higher than expected due to differential charging between the Li_2CO_3/LiOH surface layer and LLZO. As noted in the experimental methods, in addition to differential charging, using adventitious carbon in the C 1s was not a reliable referencing strategy as carbon species were mostly reduced/removed by Li deposition. As a result, Cu metal (present as an impurity in the Li) was used as a charge reference instead, with the position of Zr^{4+} in the Zr 3d spectrum then used as a charge reference for samples

without Li deposited to ensure self-consistent charge referencing for LLZO. As a result of this referencing scheme, intensities from both Li_2CO_3 and LiOH were shifted to higher binding energy, resulting in a 2 eV shift for these species in both the C 1s (Li_2CO_3) and O 1s (Li_2CO_3 and LiOH).

For unpolished surfaces, ca. 20% of the carbon intensity is related to Li_2CO_3, with a significant drop to 9.6% relative intensity after polishing, consistent with the decrease in CO_3 content observed in the O 1s spectra. Heating to 80 °C results in no significant changes to the C 1s spectrum, as Li_2CO_3 is not removed at this temperature. After heating to 500ºC, the carbonate peak disappears, further indicating that the Li_2CO_3 layer is fully removed. Adventitious carbon species are also partially removed by heating to 500ºC, as shown by the intensity drop of the remaining C 1s peak relative to the La 4s peak.

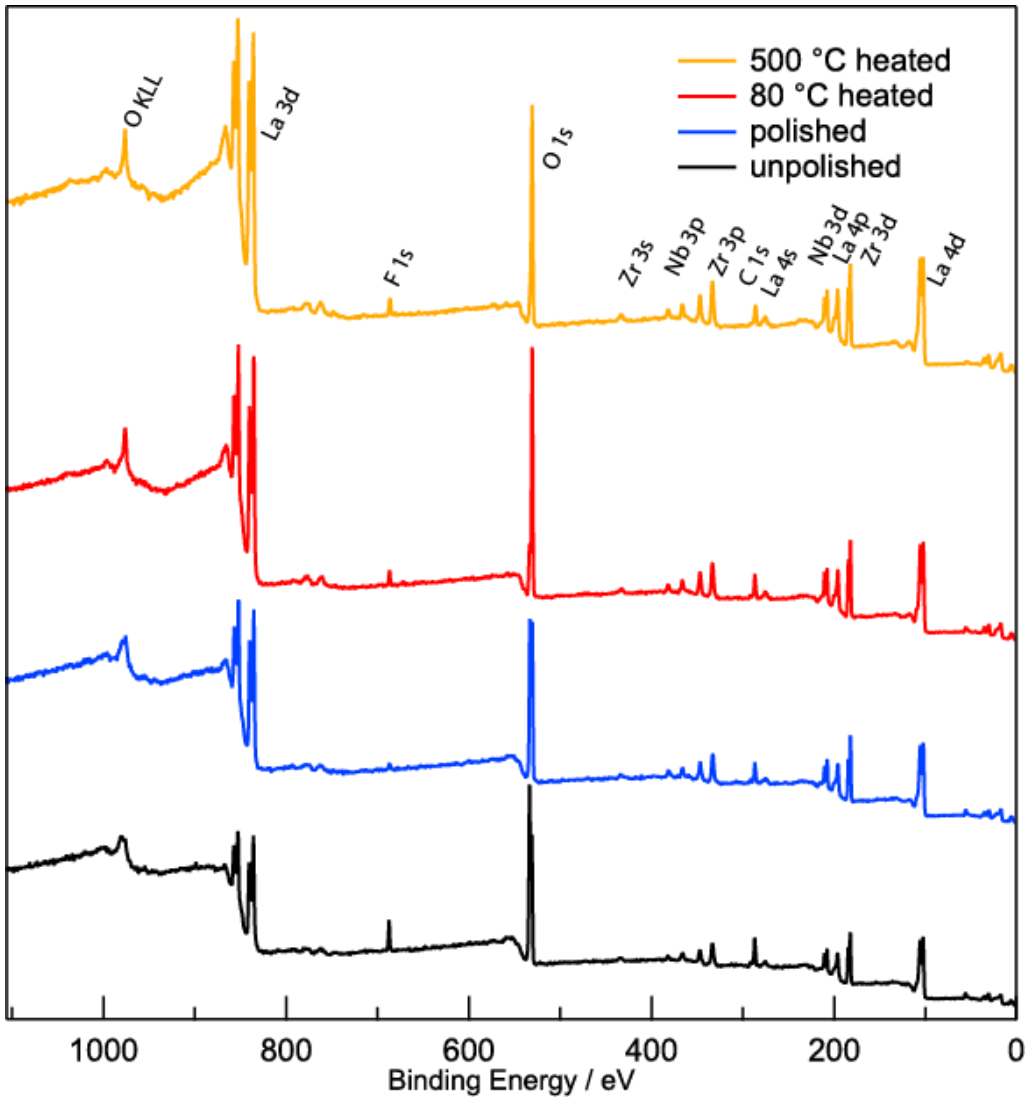

Figure S3. LLZO XPS survey spectra from unpolished, polished, 80°C UHV heated and 500°C UHV heated Nb-doped LLZO surfaces.

Figure S3 shows XPS survey spectra of four distinct surfaces (unpolished, polished, heated to 80°C and heated to 500°C in UHV) for Nb doped LLZO. Results from Al and Ta doped LLZO are similar. Generally, along with removing more surface oxidation species, the signal from bulk LLZO increases, which is most obvious for the La 3d peak in the 835 – 857 eV region.

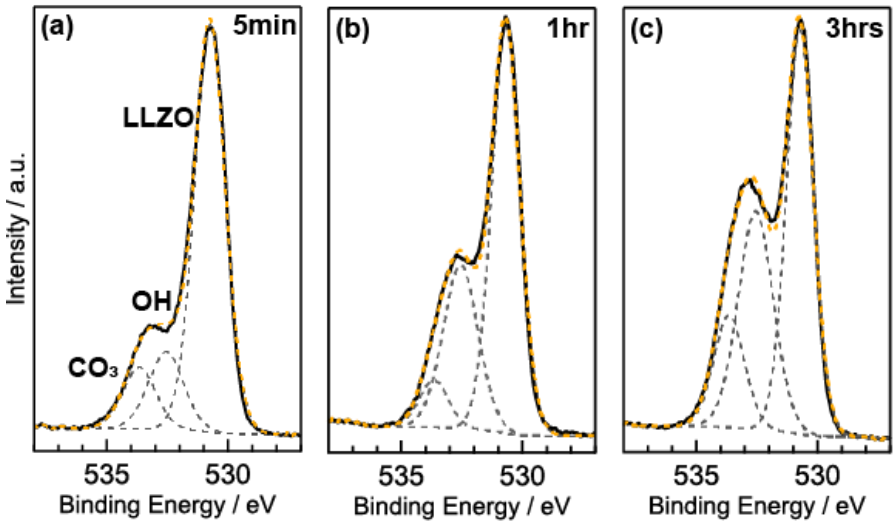

Figure S4. XPS O 1s core level spectra for annealed LLZO exposed to the glove box for (a) 5min (b) 1hr and (c) 3 hrs, showing the rapid reforming of the reaction layer and an increase in both carbonate and hydroxyl content with time.

Experiments were done to study how quickly the LLZO sample oxidizes in Ar glove box (H_2O and O_2 content $\leq$ 0.5ppm). LLZO samples annealed to 500ºC in UHV to remove all carbonate and hydroxyl species were placed in the glove box for the designated times, then transferred back into the XPS chamber to analyze the surface oxidation state. After just 5 minutes, 11% and 15% of the surface oxygen content can be assigned to carbonate and hydroxyl species, respectively, demonstrating that the surface oxidation takes place quite quickly, even in a nominally pure glovebox atmosphere. After 1 hour inside the glove box, the relative carbonate and hydroxyl peak intensities are 9% and 26%, respectively, indicating that LiOH is formed slightly faster than Li_2CO_3. After 3 hours inside of the glove box, the carbonate and hydroxyl

peak intensities both increased to 16% and 36% respectively, which is comparable to the surface composition prior to polishing.

Table S2. Deconvoluted XPS peak positions and full width at half maximum (FWHM) for Nb, Zr, O and C species shown in the manuscript.

Element/Species	**Binding Energy**		
Nb	**$3d_{5/2}$**	**$3d_{3/2}$**	**FWHM**
5+	207.9	210.6	1.08
4+	206.4	209.2	1.15
3+	205.3	208.0	1.01
2+	204.2	206.9	1.2
1+	203.2	205.9	0.94
Zr	**$3d_{5/2}$**	**$3d_{3/2}$**	**FWHM**
4+	182.4	184.8	1.16
ZrO_x	180.6	183.0	1.37
Zr^0	179.0	181.4	1.3
O	**1s**		**FWHM**
LLZO	530.7		1.29
O-C-O*	531.8		1.45
LiOH	532.9		1.5
Li_2CO_3	533.8		1.56
C	**1s**		**FWHM**
sp^3	286.8		2.06
O-C-O*	289.1		2.27
Li_2CO_3	291.7		1.62

*Note that a small amount of O-C-O content was also observed in the C 1s for both unpolished and polished LLZO samples. Fitting this species in the O 1s did not meaningfully change the quality of the fit, nor the relative OH/CO_3 content. As our focus was on the reactivity of the LLZO surface and not the composition of the adventitious carbon layer, for clarity this peak was not included in the O 1s core level fitting shown throughout.

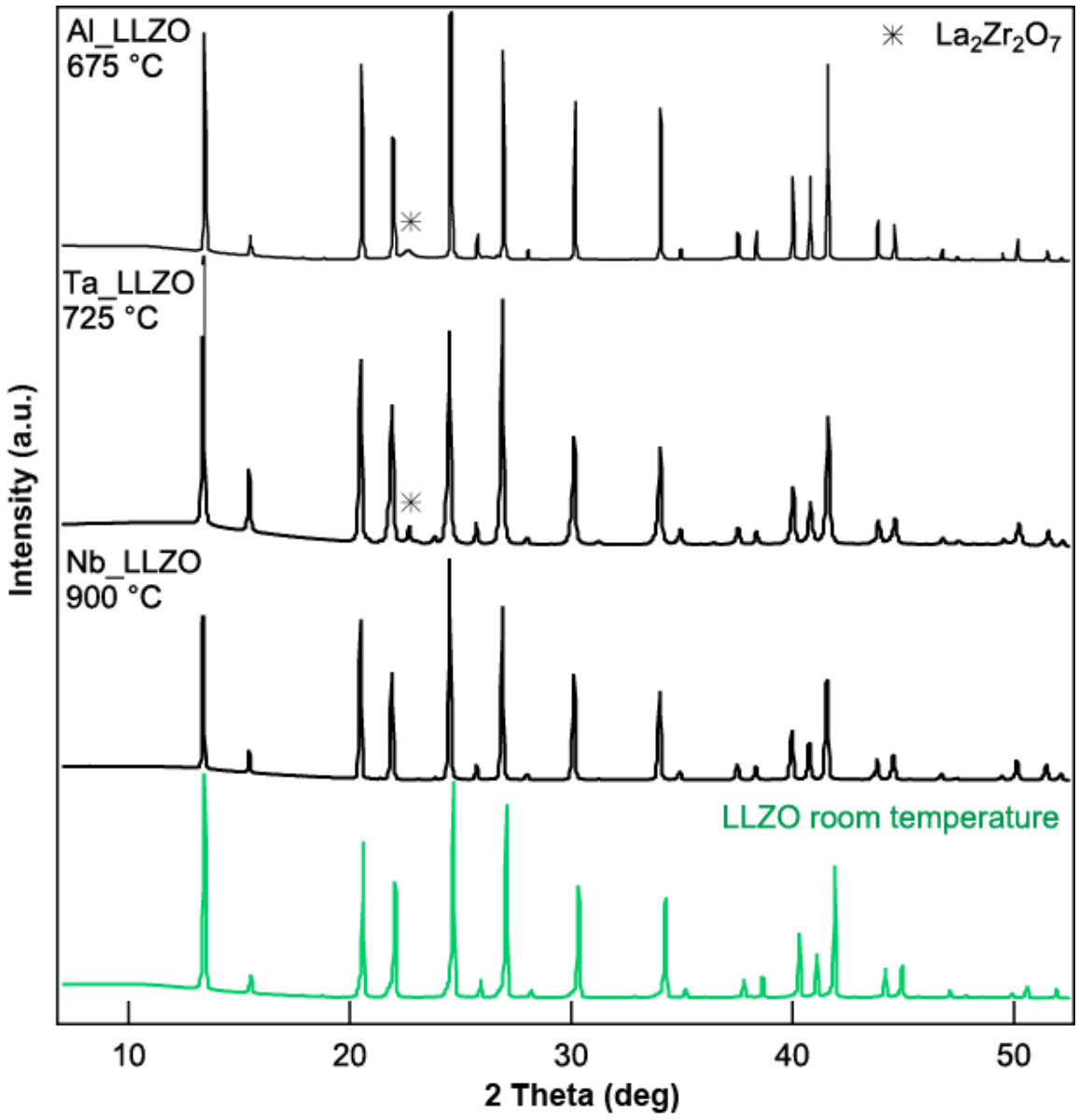

Figure S5. In situ X-ray diffraction patterns of Al-, Ta- and Nb-doped LLZO heated in high vacuum until additional peaks representing secondary phase formation were observed. Al-, Ta- and Nb-doped were observed to be stable until 675ºC, 725ºC and 900ºC, respectively. A representative pattern for LLZO measured at room temperature is also shown for comparison (green line). *Marks the $La_2Zr_2O_7$ secondary phases that formed at elevated temperature.

UHV heating was shown to be an effective way to remove surface oxidation and adsorprtion species; however, heat treatment can induce the formation of lithium-deficient $La_2Zr_2O_7$ secondary phases. In order to determine the window of structural stability during UHV annealing, we heated three pieces of Al, Ta, and Nb doped LLZO pellets up to 900 °C using the same heating rate under high vacuum conditions (10^{-8} mbar) and performed in situ X-ray diffraction using synchrotron X-rays (λ=1.25Å) at the Advanced Photon Source (APS) at Argonne National Laboratory (Figure S5). We note in all cases that the mismatch of the peaks at room temperature (green line) and high temperature (black lines) is due to lattice expansion while heating.

For all LLZO samples, pure cubic garnet phase is observed from room temperature up to 600 °C. At 675 °C, the $La_2Zr_2O_7$ phase starts to appear in Al-doped LLZO, evidenced by a growing peak at 22.5° (marked with *) due to the loss of lithium and oxygen at high temperature. Ta doped LLZO did not exhibit $La_2Zr_2O_7$ phase formation until 725°C. Surprisingly, the Nb-doped LLZO did not exhibit any $La_2Zr_2O_7$ up to 900°C, which was the highest accessible temperature in the high vacuum chamber used for in situ measurements. As 500ºC was the maximum temperature accessed in XPS heating experiments to remove surface reaction species, in situ XRD demonstrates that no lithium deficient phase formation should occur. This indicates that the subsequent reactivity observed with Li metal is intrinsic to the LLZO-Li interface, rather than the contribution of any impurity phases formed as a result of the heat treatment.

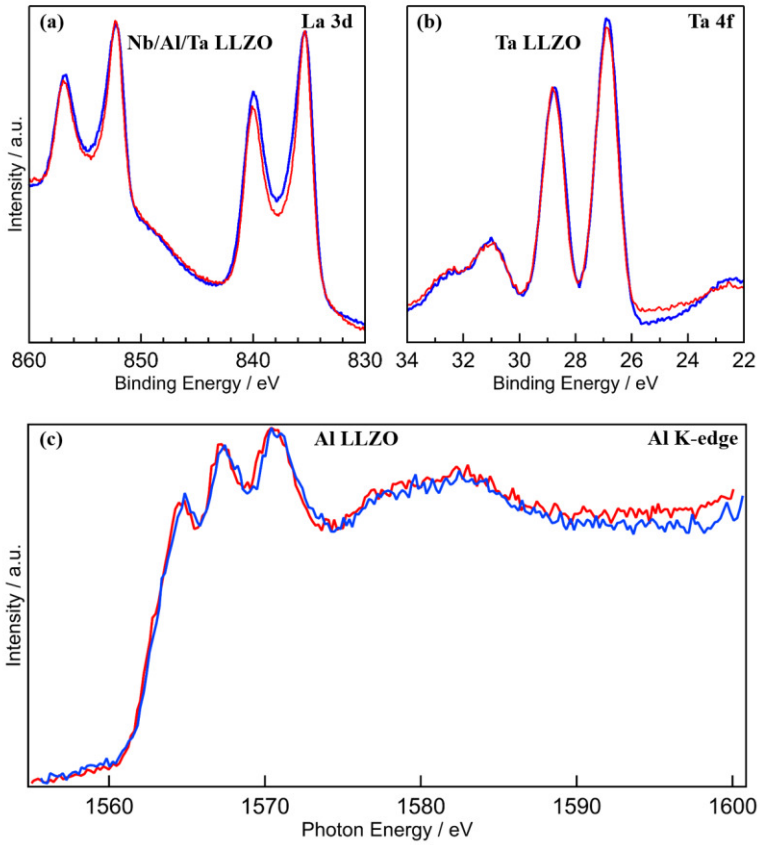

Figure S6. XPS core-level spectra from LLZO before (red) and after (blue) Li deposition reveal (a) no valence change on La for all doped LLZO samples; and (b) no valence change on Ta for Ta-doped LLZO. (c) Soft X-ray adsorption total fluorescence yield spectra on Al K-edge from Al doped LLZO before (red) and after (blue) Li deposition indicate no Al reduction in the bulk of LLZO.

Regardless of dopant type or surface treatment, no reduction of La was observed. A representative La 5d core level spectrum is shown in Fig. S6a for UHV annealed, Ta-doped LLZO. Similar to La, Ta is also stable to reduction by Li, regardless of surface treatment, as shown in Figure S6b for the same sample (UHV annealed Ta doped LLZO). The valence of Al

cannot be determined from XPS as it overlaps with the stronger Cu 3s peak from Cu impurities in the Li target; therefore, Al K-edge soft X-ray adsorption spectroscopy (XAS) was performed to rule out any bulk reduction of Al species. Li was sputtered onto polished Al doped LLZO samples, which were then transferred to the XAS chamber at the APS while protected with Ar gas. There is no shift in the Al-K edge after Li deposition, indicating that Al does not reduce in the bulk.

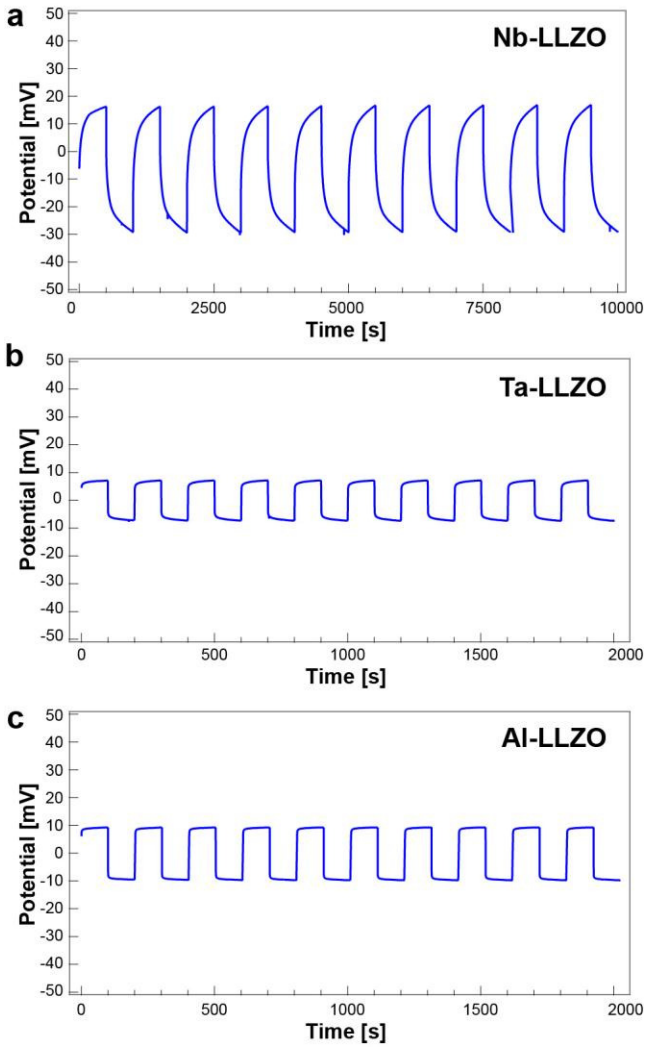

Figure S7: Galvanostatic cycling of Nb-doped (top), Ta-doped (middle), and Al-doped (bottom) LLZO at 8 μA cm^{-2} showing similar behavior of Al- and Ta-doped samples, but higher polarization and significantly longer cycle times needed to reach quasi-steady-state conditions for Nb-doped material.

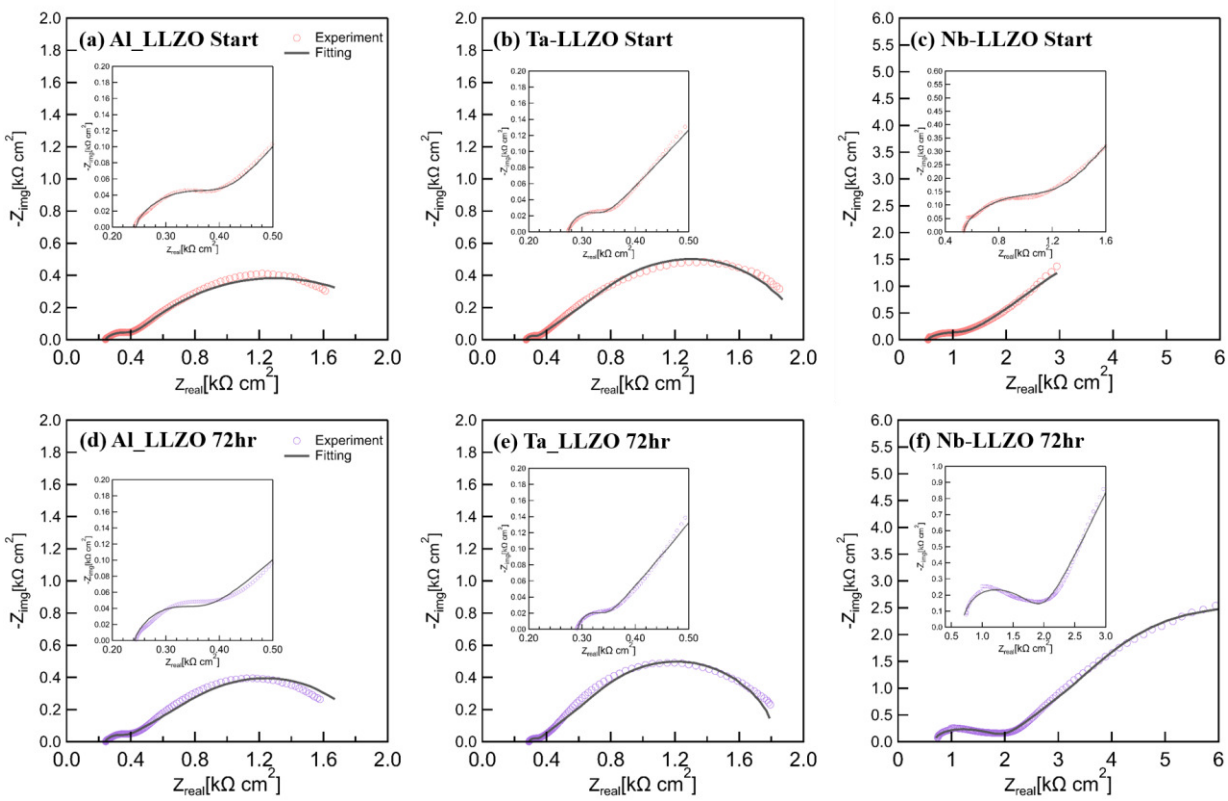

Figure S8. EIS spectra with fitting curve for Li-Li symmetric cells with (a) Al (b) Ta (c) Nb-doped LLZO after assembly and (d) Al (e) Ta (f) Nb doped LLZO after 72 hours of impedance measurement.

Table S3. Induction, resistance, capacitance and Warburg impedance values for all fittings of EIS spectra shown in Fig. S7.

Sample		L1 [μH]	R1 [Ω cm²]	R2 [Ω cm²]	C [μF]	W [Ω cm²]
Al-LLZO	Start	3.73	237.5	101.2	29.8	1574
	72 hr	3.72	240.3	113.2	39.3	1431
Ta-LLZO	Start	6.05	268.9	52.85	11.3	1693
	72 hr	6.1	287.6	44.75	9.3	1516
Nb-LLZO	Start	11.5	487.7	783.2	88.9	5288
	72 hr	16.3	334.4	1675	8.1	7185

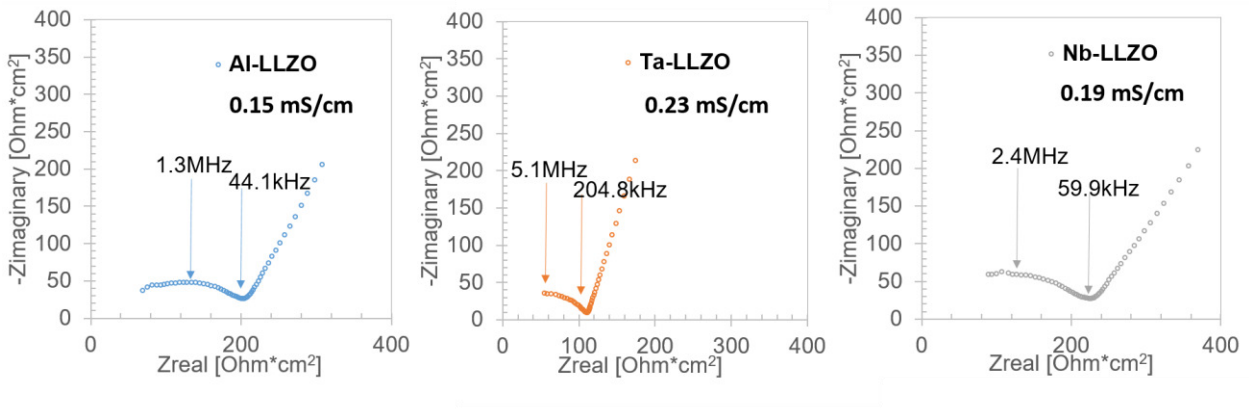

Figure S9. EIS spectra measured from 7 MHz – 250 mHz for Au||LLZO||Au cells with (a) Al (b) Ta and (c) Nb-doped LLZO. Bulk ionic conductivities (mS cm^{-1}) are calculated for each doped LLZO

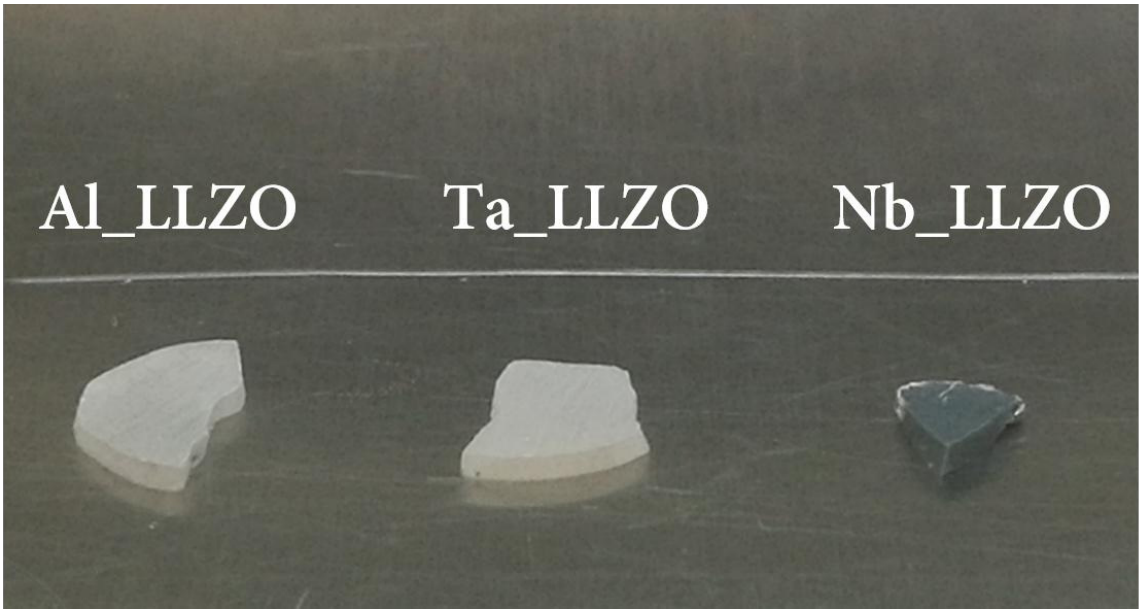

Figure S10. Photo of Al, Ta and Nb doped LLZO extracted from coin cells after 3 days of impedance measurements and polished to remove ~0.3 mm from the surface. Nb-doped LLZO shows significant discoloration, whereas Al- and Ta-doped LLZO stay the same color as before sputtering Li. As the LLZO pellets are hot-pressed in a graphite die and are semi-transparent as-synthesized, the slight gray cast to Al- and Ta-doped pellets in this photo arises from a combination of residual carbon from the hot pressing process and the color of the stainless steel base of the glove box underneath them.

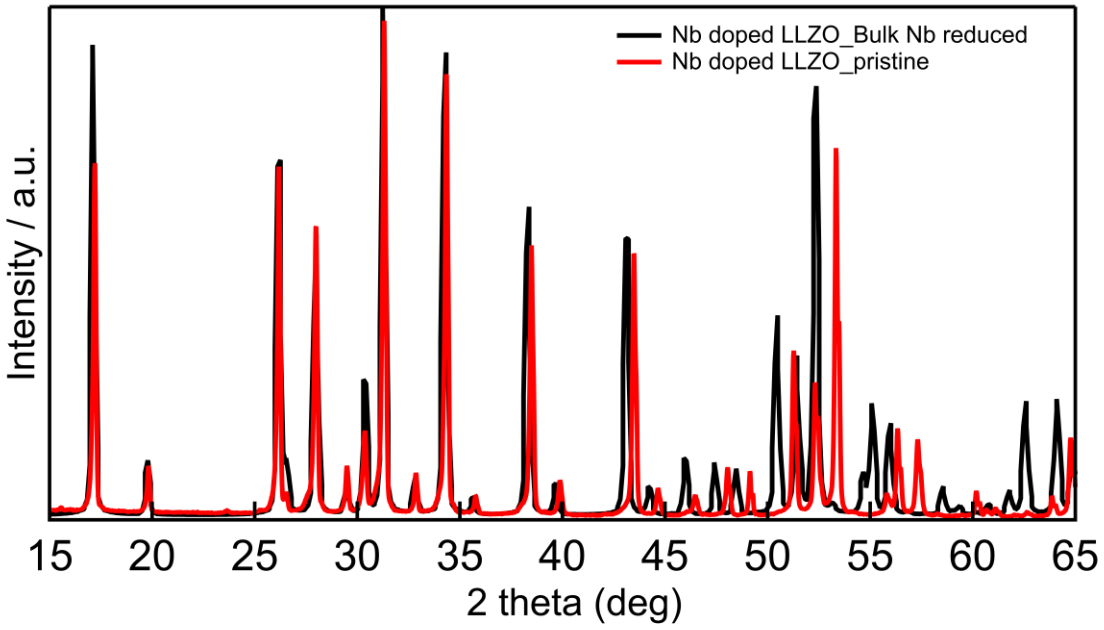

Figure S11. X-ray diffraction patterns of Nb-doped LLZO before reaction with lithium (red line) and after 3 days of reaction with lithium (black line). Shifting of the XRD peaks to lower 2θ after reaction indicates lattice expansion, which is consistent with bulk Li insertion and supports the hypothesis that Li insertion leads to Nb reduction in the bulk.

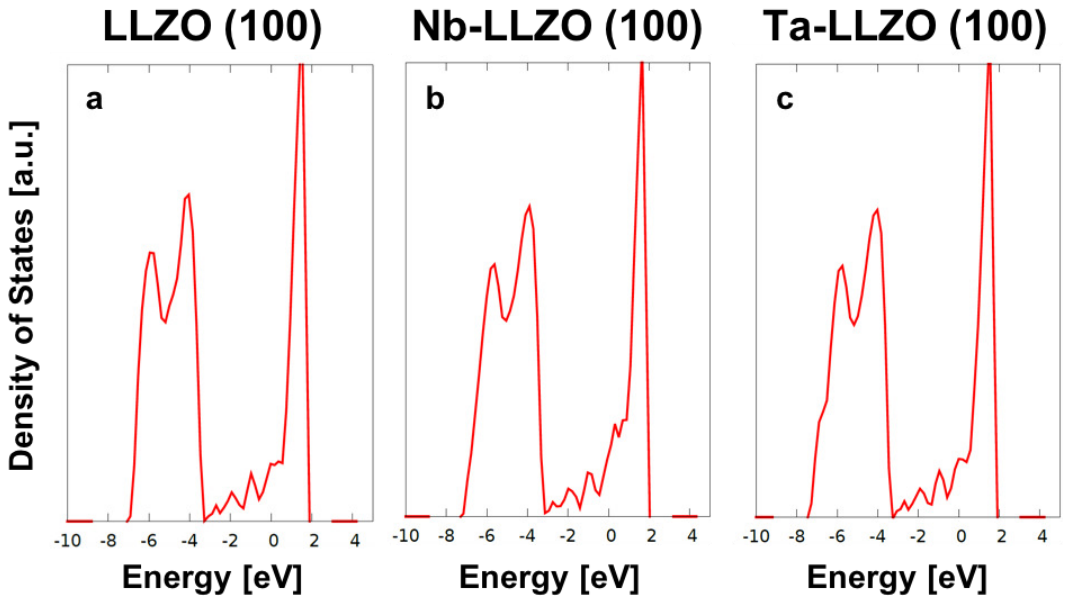

Figure S12. Densities of electronic states from DFT calculations for the interface structures of Li/LLZO with a) no dopants; b) Nb dopants and c) Ta dopants. The zero of energy is the Fermi level. Li metal states span the band gap of LLZO in all cases.

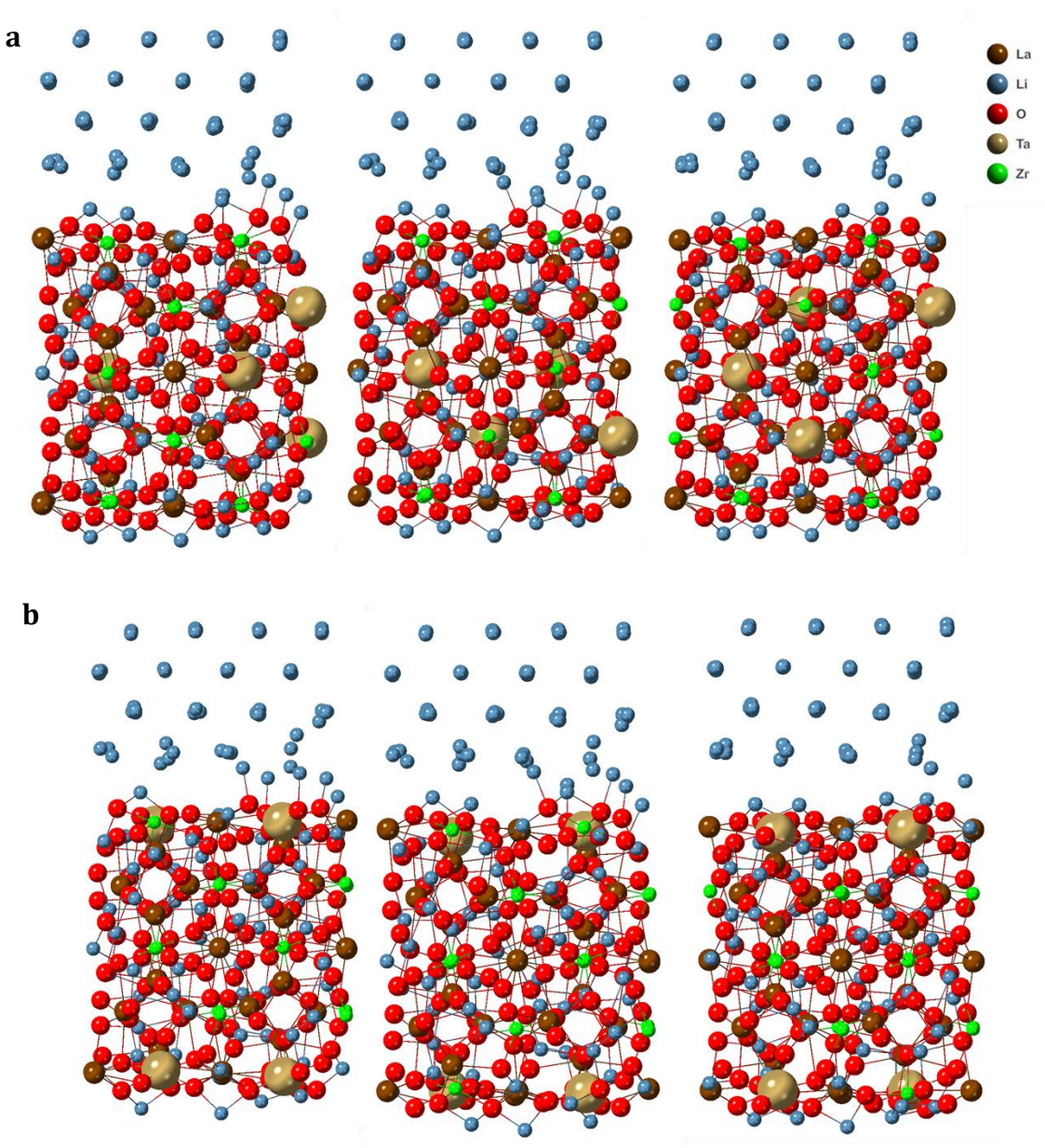

Figure S13å. DFT-calculated structures of different dopant distributions: a) examples of three different optimized structures of Ta-doped LLZO where dopant atoms are located in the "bulk" of the slab, and b) examples of three different optimized structures of Ta-doped LLZO where Ta atoms are at the surface of the slab. Ta atoms are shown as large spheres. The same initial locations were chosen for Nb dopants that were subsequently optimized (not shown).

Seeking additional insight into thermodynamic stability, we have compared differences in DFT-calculated energies for Ta and Nb in LLZO with differences in their respective oxides. We have chosen H-Nb_2O_5 structure for these calculations (Acta Cryst. (1976). B32, 764.). The Ta dopant energy relative to that of Nb dopant in LLZO bulk case is just slightly more favorable than the Ta in Ta_2O_5 relative to Nb in Nb_2O_5, by 0.04 eV/atom for the LLZO without deposited Li metal and by 0.09 eV/atom with Li metal. In the case of dopants near the surface, Ta was less stable than Nb compared to their respective oxides by 0.16 eV/atom without Li and by 0.15 eV/atom with Li. This indicates that although chemical potential differences are relatively small between Ta and Nb in LLZO in comparison to their respective pentoxides, their chemical potentials near the surface show considerable differences in favor of Nb with the same reference.